Role of $4f$ electrons in crystallographic and magnetic complexity

Arjun K. Pathak,[1,*] Durga Paudyal,[1] Yaroslav Mudryk,[1] and Vitalij K. Pecharsky[1,2]
[1]*The Ames Laboratory, U.S. Department of Energy, Iowa State University, Ames, Iowa 50011-3020, USA*
[2]*Department of Materials Science and Engineering, Iowa State University, Ames, Iowa 50011-2300, USA*
(Received 21 June 2017; published 9 August 2017)

The functionality of many magnetic materials critically depends on first manipulating and then taking advantage of highly nonlinear changes of properties that occur during phase transformations. Unique to lanthanides, property-defining $4f$ electrons are highly localized and, as commonly accepted, play little to no role in chemical bonding. Yet here we demonstrate that the competition between $4f$-electron energy landscapes of Dy ($4f^9$) and Er ($4f^{11}$) is the key element of the puzzle required to explain complex interplay of magnetic and structural features observed in $Er_{1-x}Dy_xCo_2$, and likely many other mixed lanthanide systems. Unlike the parent binaries—$DyCo_2$ and $ErCo_2$—$Er_{1-x}Dy_xCo_2$ exhibits two successive magnetostructural transitions: a first order at T_C, followed by a second order in the ferrimagnetically ordered state. Supported by first-principles calculations, our results offer new opportunities for targeted design of magnetic materials with multiple functionalities, and also provide a critical insight into the role of $4f$ electrons in controlling the magnetism and structure of lanthanide intermetallics.

DOI: 10.1103/PhysRevB.96.064412

I. INTRODUCTION

Lanthanides (Ln) and their compounds are favored by the condensed matter physics, solid state chemistry, and materials science communities because of characteristic physical and chemical properties that arise from systematic changes in their $4f$ shells (although ironically, the namesake—lanthanum—has no $4f$ electrons). The highly localized $4f$ states are responsible for the local magnetic moments associated with the majority of Ln^{3+} ions. Unlike itinerant $3d$, $4f$ electrons couple via indirect exchange interactions [1] mediated by the delocalized $5d$ [1] and $6s$ [2] states. The spin polarization and exchange splitting that result lead to measurable itinerant (mainly $5d$) magnetism [2].

The role of $4f$ electrons in determining physical properties of lanthanide-containing materials is well known. Their influence on the chemistry of alloys and intermetallics is, however, obscured by the fact that the occupied $4f$ states are buried deep below the Fermi level (E_F) and are well separated from the unoccupied $4f$ states far above E_F. Hence, when the crystal structure of a material changes due to a substitution of one lanthanide for another, it is seldom assumed to be related to changes in $4f$ bonding. As a matter of fact, Laves phases [3] that are central to this work epitomize dominance of the geometric over the electronic factors in controlling phase stability and structure selection [4]. Here, we show that ignoring the $4f$ states leads to a far from complete picture that does not correctly describe neither the ground nor the metastable crystal and magnetic phases, nor their transformations and interplay in these lanthanide containing compounds.

A number of rare-earth (Sc, Y, and Ln) compounds are known to strongly respond to varying magnetic field (H), pressure (p), temperature (T), or composition (x) by exhibiting structural or/and magnetic phase transformations. A substantial number of seemingly different systems, including itinerant electron metamagnetic [5], geometrically frustrated [6], and molecular liquids [7], may show powerful responsive behaviors. The latter—the unusually strong sensitivity of materials to minor external influences—goes far beyond basic science. Mastering phase transformations without major hysteresis losses is critical for intelligent design of energy conversion materials, e.g., those suitable for caloric cooling [8,9]. Among lanthanide-based intermetallics, the so-called Laves phases RM_2 (R = rare-earth, $M = 3d$ transition metals) [10,11] exhibit a range of interesting physical behaviors that arise from the interactions between the localized $4f$ and itinerant $3d$ electrons. These compounds crystallize in one of the three closely related structures: hexagonal $MgZn_2$ type, also known as C14; cubic $MgCu_2$ type (C15); and hexagonal $MgNi_2$ type (C36); but it is mostly the compounds with the C15 structure that show unusual sensitivity to external stimuli (x, p, H, and T). In many cases, these compounds experience structural distortions at low temperatures, which are usually coupled with magnetic ordering/reordering transformations [12].

Magnetism of binary RCo_2 compounds is strongly dependent on the nature of the R element. Consider three neighboring lanthanides, for example, Dy, Ho, and Er. $DyCo_2$ and $ErCo_2$ undergo first-order cubic-to-tetragonal and cubic-to-rhombohedral magnetostructural transitions, respectively, upon cooling. The change in the unit cell volume ($\Delta V/V$) at the Curie temperature, T_C, of $DyCo_2$ is much smaller compared to $ErCo_2$ [13] and the application of magnetic field easily suppresses the volume discontinuity in $DyCo_2$, leading to a second-order phase transition when $H > 0$ [14,15]. On the other hand, the first-order transition is preserved in $ErCo_2$ even at $H = 40$ kOe [13]. $HoCo_2$ is a special case, where the compound exhibits two successive transformations: a first-order cubic to tetragonal at T_C, and a second-order distortion coupled with spin reorientation that lowers symmetry further from the tetragonal to orthorhombic leading to $Fddd$ space group symmetry via a rearrangement of both $3d$ states of Co and $5d$ states of Ho [16].

Although binary RCo_2 intermetallic compounds have been broadly studied over the last few decades, the magnetic and crystallographic behaviors of pseudo-binary $R_{1-x}R'_xCo_2$ have not received much attention. Simultaneously, $4f$-$3d$

*Corresponding author: pathak138@ameslab.gov

interactions have been scrutinized, driven by their technological relevance in a concerted effort to develop stronger R-Co permanent magnets, while $4f^{R'}$-$4f^{R}$ interplay was basically overlooked. Thus, much of the interesting fundamental science, especially considering the localized nature of $4f$ electrons and possible functionality of mixed lanthanide materials, remains unexplored despite a recent surge of interest in rare-earth materials [17]. Present lack of basic understanding in turn impedes future rational design of materials that undergo first-order structural transformation with controlled hysteresis. Here we present our recent findings in understanding the ground-state magnetism and crystal structure in a simple model—a mixed rare-earth intermetallic system that undergoes a truly unusual sequence of phase transformations that has never been reported and understood, in spite of a long history of examination of similar systems.

II. EXPERIMENT

A. Synthesis

The polycrystalline $Er_{1-x}Dy_xCo_2$ samples with $x = 0.05$, 0.25, 0.40, 0.50, 0.75, and 0.95 weighing ~5 g each were prepared by arc melting of stoichiometric amounts of the constituent elements in an argon atmosphere on a water-cooled copper hearth. The Er and Dy metals were obtained from the Materials Preparation Center of the Ames Laboratory [18]. The Er was 99.98 + wt.% (99.85 + at.%) pure, and the Dy – 99.98 + wt.% (99.82 + at.%) pure with respect to *all other elements* in the periodic table. The Co metal of 4N purity was purchased from Alfa Aesar Inc. The samples were remelted 3 to 4 times flipping over after each melting to ensure homogeneity. The weight losses after the melting were less than 1%, thus the nominal compositions were accepted as the actual ones. Since both of the parent compounds form via shallow peritectic reactions, the as-cast alloys were heat treated at 800 °C for 7 days. The heat treated materials were used in all experiments.

B. X-ray crystallography

The room-temperature crystal structure and phase purity were determined using x-ray powder diffraction (XRD) experiments carried out on a PANalytical X'Pert PRO diffractometer. The x-ray powder diffraction measurement as a function of temperature between 5 and 300 K in a zero magnetic field was carried out on a Rigaku TTRAX rotating anode powder diffractometer employing Mo K_α radiation. Further details about sample preparation and experimental setup for temperature-dependent x-ray diffraction can be found in Ref. [19]. Structural parameters were determined by Rietveld analysis using LHPM Rietica [20].

C. Magnetization and heat capacity measurements

Direct current (dc) magnetization was measured in a superconducting quantum interference device magnetometer (SQUID, MPMS-XL7, Quantum Design). Alternating current (ac) magnetic susceptibility was measured in a driving ac field of 1 Oe using SQUID magnetometer at frequencies ranging from 1 Hz to 1 kHz in zero applied dc field. Heat capacity measurements were performed using a homemade adiabatic heat-pulse calorimeter [21] and a physical property measurement system (PPMS, Quantum Design).

D. *Ab initio* calculation

The local spin density approximation including Hubbard U (LSDA + U) [22] approach has been employed to support and rationalize experimentally observed magnetostructural behaviors of $Er_{1-x}Dy_xCo_2$ compounds. The LSDA + U is implemented in the tight-binding linear muffin-tin orbital (TB-LMTO) [23] and full-potential linear augmented plane-wave (FP-LAPW) [24] methods. The orbital-dependent Coulomb and exchange interactions in LSDA + U remove the degeneracy, and the $4f$ states split in different energy locations as prescribed by the tetrahedral site symmetry of R atoms, octahedral local symmetry of Co atoms, and the number of partially filled orbitals in both spin channels obeying the Hund's spin and orbital rules in the Laves phase structure of these compounds. Here, the spin-orbit coupling of the $4f$ states ($J = L + S$, for the heavy lanthanides) follows the Hund's rule. The electronic structure calculations performed with different values of Hubbard U ranging from 1 to 7 eV indicate that with the higher values of the U, the occupied $4f$ states are shifted to the lower energy while the unoccupied $4f$ states are shifted to the higher energy, as expected. A total of 145 special k points in the irreducible part of the Brillouin zone have been used for k-space integration, which was sufficient for convergence of total energies, magnetic moments, and $4f$ and d splitting.

The electronic structure calculations were performed by reducing the cubic ($Fd\bar{3}m$), tetragonal ($I4_1/amd$) and orthorhombic (*Fddd* and *Imma*) symmetries of different $Er_{1-x}Dy_xCo_2$ phases to P1. Then, depending upon the concentration, Er and Dy atoms were randomly placed into the eight (cubic) or four (tetragonal and orthorhombic) R sites that are no longer formally connected by any symmetry other than lattice translations [25]. Hence, to model cubic $Er_{0.75}Dy_{0.25}Co_2$, six Er and two Dy atoms were randomly placed in eight R positions inside a triclinic unit cell with $a = b = c$ and $\alpha = \beta = \gamma = 90^\circ$ that has the same unit cell volume as the cubic cell. Because of the localized nature of the $4f$ electrons, different random placements of six Er and two Dy atoms in 28 possible models of $Er_{0.75}Dy_{0.25}Co_2$ show identical local $4f$ crystal-field splitting and the local magnetic moments. This indicates that the actual placement of Er and Dy atoms in the triclinic unit cell has little to no effect on the calculated magnetic properties of $Er_{0.75}Dy_{0.25}Co_2$, assuming collinear ferromagnetism between Er and Dy and ferrimagnetism between R and Co atoms.

III. RESULTS AND DISCUSSION

A. Magnetism

The zero-field-cooled (ZFC) warming, field-cooled cooling (FCC), and field cooled-warming (FCW) magnetization data for $Er_{1-x}Dy_xCo_2$ ($0.05 \leqslant x \leqslant 0.95$) measured at $H = 100$ Oe are shown in Figs. 1(a)–1(f). Considering that the Co $3d$ moments (~1 μ_B/Co) couple antiparallel to the lanthanide moments in RCo_2 [26], all transitions at T_C are ferrimagnetic.

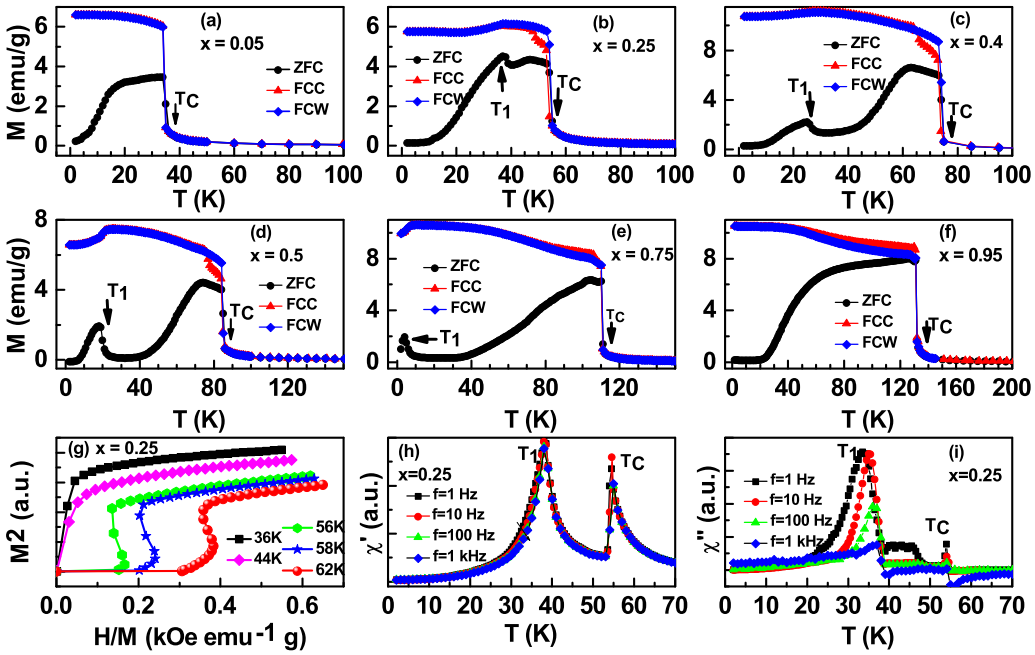

FIG. 1. Magnetization measurements. (a)–(f) Zero-field-cooled (ZFC) warming, field-cooled cooling (FCC), and field-cooled warming (FCW) magnetization of $Er_{1-x}Dy_xCo_2$ alloys measured in $H = 100$ Oe. (g) Arrott plots in the vicinity of phase transitions. Temperature dependence of real (h) and imaginary (i) components of ac magnetic susceptibility for $x = 0.25$ measured in a driving ac field of 1 Oe and frequencies from 1 to 1000 Hz.

For the end compositions with $x = 0.05$ and 0.95, lone phase transitions observed at T_C are consistent with the pure binaries. As shown in Fig. 1, additional phase transitions (labeled T_1) occur below T_C when $0.25 \leqslant x \leqslant 0.75$. Splitting of the ZFC and FCC curves is due to pinning of domain walls, however, there is also an unexpected splitting of the FCC and FCW curves right below the T_C. The splitting is likely related to a different kinetics of the first-order phase transition when the system traverses a phase-separated state (phase coexistence) during cooling (FCC) and heating (FCW), in which concentration of one phase increases/decreases at the expense of another [27]. At the same time, this thermomagnetic irreversibility is observed only in a low magnetic field (100 Oe), being suppressed by a 10 kOe magnetic field (not shown). The 10 kOe field can be sufficient to suppress the irreversibility related to domain wall dynamics, but is not likely to completely remove the phase coexistence [28,29]. Thus the observed effect is likely related to different domain structures associated with two crystallographically distinct phases—tetragonal and orthorhombic, also considering that the domain wall stability must be sensitive to strain varying differently upon cooling compared to heating.

The Arrott plot [30] shown in Fig. 1(g) suggests a first-order nature of the phase transition at T_C and the second order for transition at T_1 for $Er_{0.75}Dy_{0.25}Co_2$. Two clear maxima obtained in real (χ') and imaginary (χ'') components [Figs. 1(h)–1(i)] of the ac magnetic susceptibility for $x = 0.25$ are both consistent with dc magnetization: the peak temperatures are $T_C = 54.5$ K and $T_1 = 38$ K, matching the temperatures obtained from the first derivatives of $M(T)$ data of Fig. 1. As shown in Fig. 1(i), energy losses exhibit clear frequency dependence, suggesting one or several possible factors playing a role: spin frustration, domain wall pinning, competition of single ion anisotropies, or/and crystal-field. We note that the maximum of χ'' at T_1 shifts toward higher temperatures as the frequency increases [Fig. 1(i)], while the maximum at T_C remains at the same temperature at all measured frequencies, indicating a frustrated state between T_1 and T_C.

B. Temperature-dependent crystallography

In order to understand the low-temperature (LT) phase transformations, LT x-ray powder diffraction measurements were performed for $Er_{0.75}Dy_{0.25}Co_2$ and $Er_{0.5}Dy_{0.5}Co_2$ from 300 K down to 5 K on a Rigaku TTRAX system with a rotating anode generating Mo K_α radiation [19]. Both compounds exhibit first-order structural transformations at T_C from the cubic $Fd\bar{3}m$ to the tetragonal $I4_1/amd$ polymorphs (Fig. 2), which is visualized by splitting of their cubic (008) Bragg peaks into tetragonal (440) and (008) reflections in Figs. 2(a) and 2(b) and verified by Rietveld refinement (Table I). These transformations are basically identical to that observed in the binary $DyCo_2$ [14] and the volume changes at the first-order transition in both compounds are practically the same ($\Delta V/V = 0.29\%$). Somewhat unexpectedly, even in the alloy with 75 at.% Er the cubic to tetragonal transition at T_C resembles $DyCo_2$ even if binary $ErCo_2$ distorts rhombohedrally. However, the presence of both Er and Dy leads to a second structural distortion below T_C—from the tetragonal to orthorhombic—in $Er_{0.75}Dy_{0.25}Co_2$. Naïvely, such behavior is completely unexpected considering that the difference between Dy and Er lies in their 4f shells buried deep in the cores, and it is generally accepted that 4f electrons of different lanthanides do not hybridize directly. Yet, $Er_{0.75}Dy_{0.25}Co_2$ following the sequence of structural

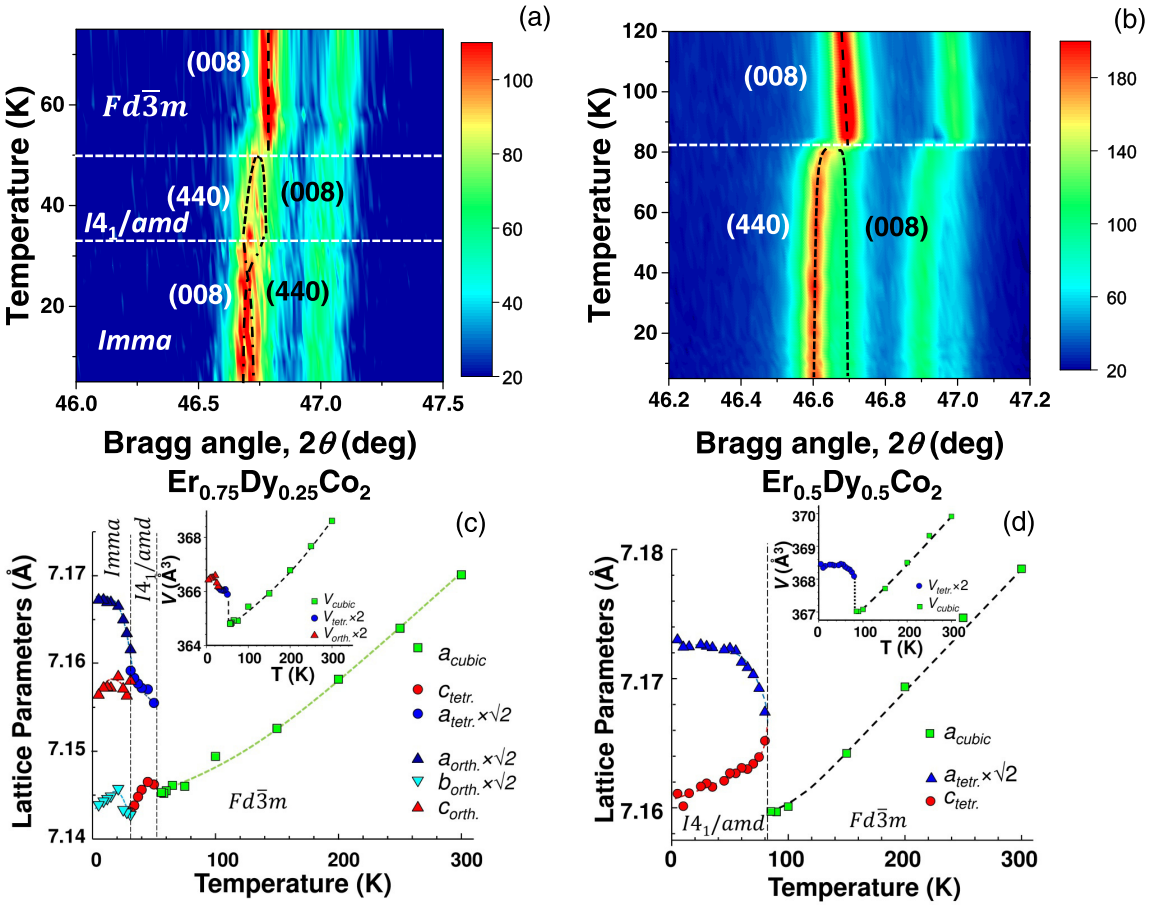

FIG. 2. Temperature dependent x-ray diffraction. (a) Temperature-induced splitting of the cubic (008) Bragg reflection into (a) (440) and (008) tetragonal and orthorhombic reflections in the $Er_{0.75}Dy_{0.25}Co_2$ phase, (b) (440) and (008) tetragonal reflections in the $Er_{0.5}Dy_{0.5}Co_2$ phase. Temperature dependence of the lattice parameters and unit-cell volume (insets) for (c) $Er_{0.75}Dy_{0.25}Co_2$, and (d) $Er_{0.5}Dy_{0.5}Co_2$ phases. All data are for cooling starting from 300 K.

distortions typical of $HoCo_2$ (cubic to tetragonal and then tetragonal to orthorhombic) serves as a solid evidence that collectively $4f^9$ states of Dy and $4f^{11}$ states of Er play a role and, therefore, closely resemble behavior of $4f^{10}$ states of Ho. The likely scenario, therefore, is unusually strong $4f$-$5d$-$3d$ hybridization (also see the *ab initio* calculations below).

According to the Rietveld analysis of the XRD patterns, the symmetry of the ground-state structure of $Er_{0.75}Dy_{0.25}Co_2$ is body-centered *Imma* (Table I), in which Co atoms are split into two sites and are no longer symmetrically equivalent. This is indeed unique among other RCo_2 systems which adopt ground-state *Fddd* symmetry [16], where the Co atoms remain symmetrically equivalent just like in both the cubic and

TABLE I. Crystal structures of cubic (at 300 K), tetragonal (at 45 K), and orthorhombic (at 9 K) polymorphs of $Er_{0.75}Dy_{0.25}Co_2$ as determined by Rietveld analysis of temperature-dependent x-ray powder diffraction data. The rare-earth positions (R) are occupied by 95% (3/4Er + 1/4Dy mixture), Co positions are 100% occupied.

Atom	Wyckoff & multiplicity	x/a	y/b	z/c	B_{iso}, Å^2
	Cubic, SG $Fd\bar{3}m$, $a = 7.1699(1)$ Å, $T = 300$ K				
R	8b	0.375	0.375	0.375	0.84(2)
Co	16c	0	0	0	0.93(3)
	Tetragonal, SG $I4_1/amd$, $a = 5.0606(1)$ Å, $c = 7.1463(2)$ Å, $T = 45$ K				
R	4b	0	0.25	0.375	0.35(1)
Co	8c	0	0	0	0.46(2)
	Orthorhombic, SG *Imma*, $a = 5.0678(2)$ Å, $b = 5.0516(2)$ Å, $c = 7.1567(4)$ Å, $T = 9$ K				
R	4e	0	0.25	0.3760(4)	0.38(1)
Co1	4a	0	0	0	0.8(1)
Co2	4d	0.25	0.25	0.75	0.4(1)

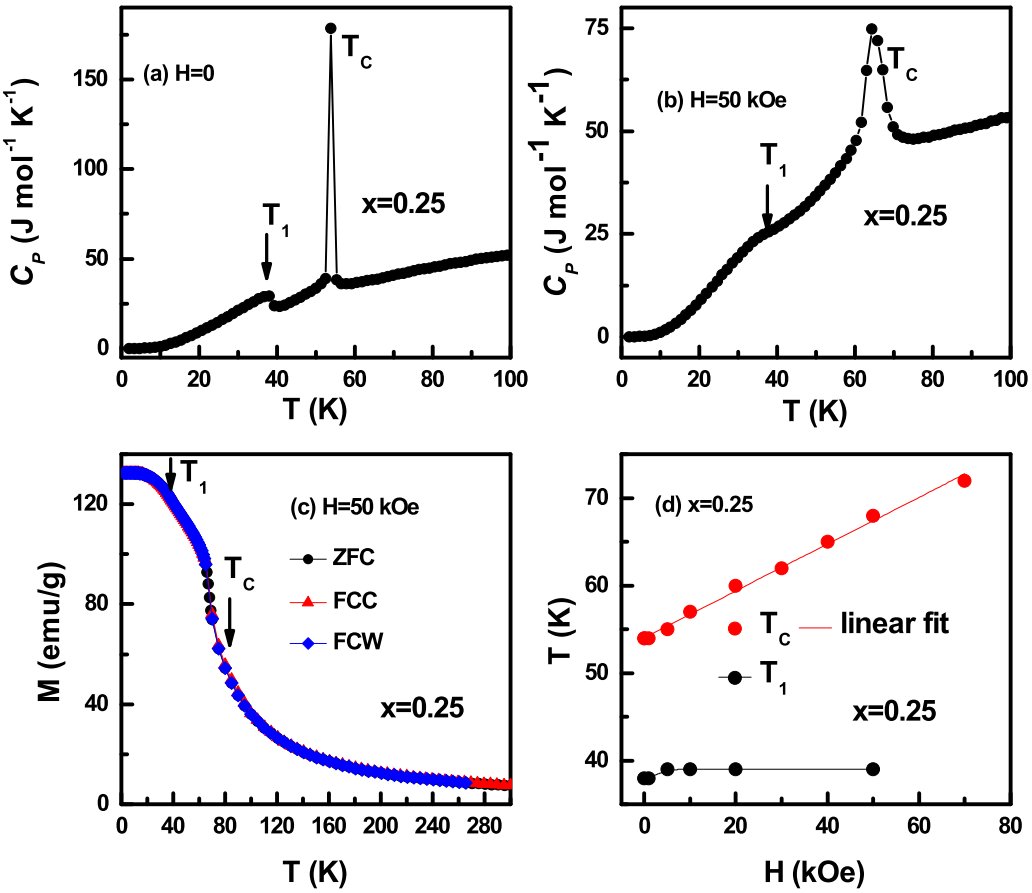

FIG. 3. Specific heat and magnetization measurements. Heat capacity C_p of $Er_{0.75}Dy_{0.25}Co_2$ measured at (a) $H = 0$ and (b) 50 kOe. (c) Zero-field-cooled (ZFC) warming, field-cooled cooling (FCC), and field-cooled warming (FCW) magnetization of $Er_{0.75}Dy_{0.25}Co_2$ measured in $H = 50$ kOe. (d) Phase transition temperatures as functions of magnetic field obtained from heat capacity measurements.

tetragonal polymorphs. Effectively, at the second critical temperature located below T_C (i.e., T_1), the tetragonal distortion is reduced—(008) and (440) Bragg peaks move closer together—as seen in Fig. 2(a). At the same time, the observed splitting of the (222) peak (not shown) at T_1 indicates the emergence of the *Imma* distortion in $Er_{0.75}Dy_{0.25}Co_2$. We note that in $HoCo_2$ the splitting of the (222) Bragg reflection does not occur at the orthorhombic transformation (hence *Fddd* space group). Rietveld refinement consistently indicates a major reshuffle of the lattice parameters at the second-order transformation: the c lattice parameter of the orthorhombic phase is nearly the same as the a parameter of the tetragonal phase, while the basal plane parameter of the tetragonal phase splits into a and b parameters in the *Imma* structure [Figs. 2(a) and 2(c)]. At the same time, $Er_{0.5}Dy_{0.5}Co_2$ alloy shows a more traditional behavior [Figs. 2(b) and 2(d)]: the tetragonal deformation occurs at T_C and this phase remains stable down to the lowest measured temperature, 5 K. The first-order nature of the ferrimagnetic transition observed at T_C is also confirmed from the corresponding significant volume change [Figs. 2(c) and 2(d), insets] and anomalies observed in heat capacities (Fig. 3).

C. Heat capacity

In agreement with the magnetization data, heat capacities of samples with $x = 0.05$ and 0.95 exhibit only one peak at T_C (not shown). Additional λ-like phase transitions are observed at T_1 for $0.25 \leqslant x \leqslant 0.75$ (Fig. 3). In a zero magnetic field, the heat capacity of $Er_{0.75}Dy_{0.25}Co_2$ indicates a strongly first-order phase transition at T_C and a second-order one at T_1 [Fig. 3(a)]. Both anomalies remain clearly distinguishable at $H = 50$ kOe, and the transition at T_C remains first order in nature, even though the corresponding heat capacity peak is substantially broadened [Fig. 3(b)], and there is no hysteresis between the FCC and FCW $M(T)$ data measured at 50 kOe [Fig. 3(c)]. We note that absence of hysteresis in first-order phase transitions is critically important for potential applications such as magnetocaloric cooling [29]. The magnetic ordering temperature increases linearly with field [Fig. 3(d)], which is typical for first-order ferromagnetic/ferrimagnetic to paramagnetic transitions, while the magnetic field dependence of T_1 is virtually nonexistent. This behavior is different from $HoCo_2$ [16], where temperatures of both transitions are increasing with rising magnetic field. The maxima of the magnetocaloric effect—property that is critical for the emerging solid-state magnetocaloric refrigeration technology—calculated from the heat capacity data are: $\Delta S_M = -15.5\,J\,kg^{-1}\,K^{-1}$ at T_C and $-5.2\,J\,kg^{-1}\,K^{-1}$ at T_1, and $\Delta T = 5.8$ and 2.2 K, respectively, for $\Delta H = 50$ kOe.

D. *Ab initio* calculations

The substantially lower energy of the tetragonal $Er_{0.75}Dy_{0.25}Co_2$ structure (by 402.5 meV/cell) compared to

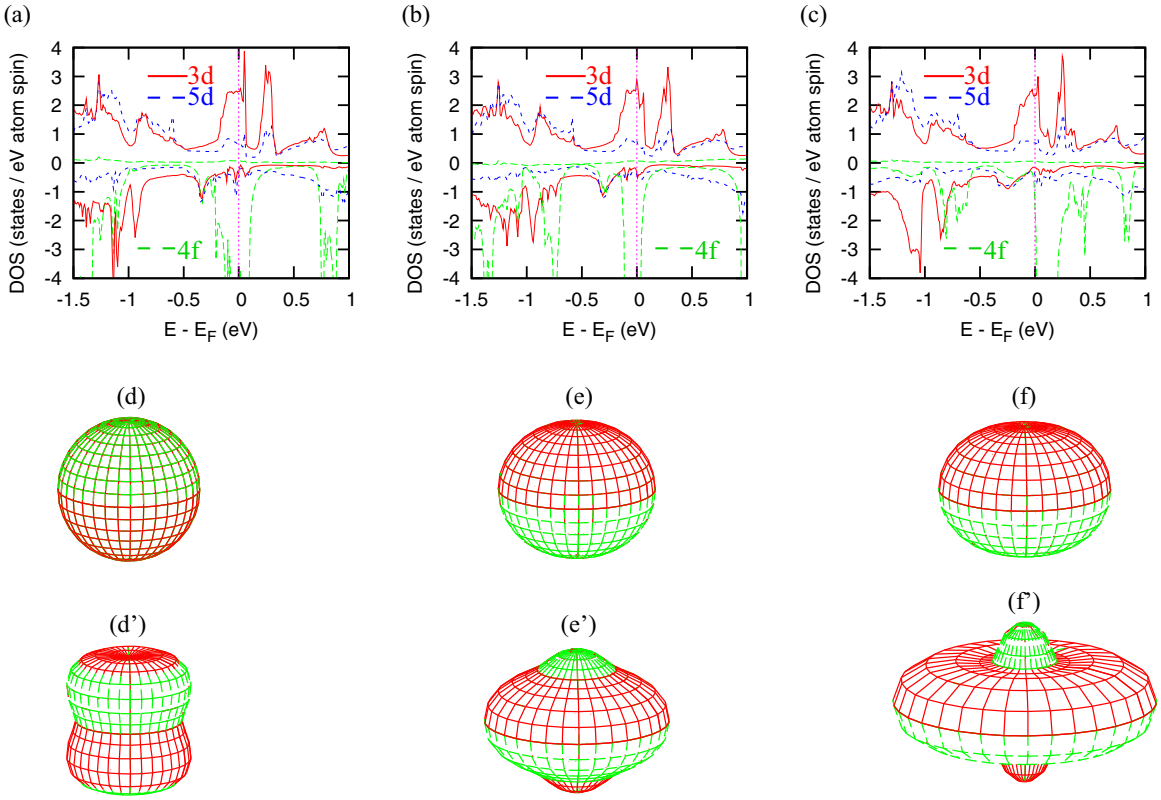

FIG. 4. First-principles calculations and $4f$ charge density. The $3d$, $5d$, and $4f$ density of states of the cubic (a), tetragonal (b), and orthorhombic *Imma* (c) structures of $Er_{0.75}Dy_{0.25}Co_2$. The $5d$ DOS are arbitrarily multiplied by 5 to visualize hybridization with $3d$ and $4f$ states. The anisotropic energy landscapes of $Er_{0.75}Dy_{0.25}Co_2$, $Er_{0.5}Dy_{0.5}Co_2$, and $Er_{0.25}Dy_{0.75}Co_2$ calculated using the anisotropic energy density expansion by employing second-order only [(d)–(f)] and both second- and fourth-order [(d')–(f')] anisotropy coefficients.

the cubic structure indicates higher stability of the former over the latter. The total energy lowers further by 11.1 meV/cell in the *Imma*-type orthorhombic structure, confirming the ground-state structure observed experimentally. A similar cubic to tetragonal to orthorhombic phase transformation sequence occurs in $HoCo_2$ [16], while a direct cubic to orthorhombic transformation has been observed in $HoAl_2$ [25]. The symmetry of the orthorhombic structure in both cases is higher and corresponds to *Fddd* group. In $Er_{0.75}Dy_{0.25}Co_2$, however, the splitting of the Co site lowers the total energy giving preference to the *Imma* structure over the *Fddd* one, which is in contrast to $HoCo_2$.

The spin down $4f$ densities of states (DOS), which are degenerate at the Fermi level and unstable in the high-symmetry cubic structure [Fig. 4(a)], are split (at ~ -0.75 and ~ 0 eV) by the tetragonal distortion [Fig. 4(b)]. The state at ~ -0.75 eV splits further and the states close to the Fermi level are pushed towards higher energy in the *Imma*-type structure making it a stable ground state [Fig. 4(c)]. The DOS calculations with the *Fddd* type orthorhombic structure, on the other hand, show $4f$ DOS similar to the cubic structure. The $4f$ spin moments of Dy and Er increase from 4.67 μ_B to 4.79 μ_B and decrease from 2.61 μ_B to 2.58 μ_B, respectively, when the cubic $Er_{0.75}Dy_{0.25}Co_2$ transforms to the tetragonal structure. The spin-down DOS near the Fermi level must be pushed towards the higher energy to achieve higher moments but such a shift is forbidden due to the crystal-field splitting. The $4f$ spin moment of Dy remains unchanged but that of Er increases from 2.58 μ_B to 2.76 μ_B when the tetragonal $Er_{0.75}Dy_{0.25}Co_2$ transforms further to the *Imma* orthorhombic. Therefore small but significant moment increase of Dy is associated with the stable tetragonal structure while the stability of the orthorhombic structure is accompanied by the increase in Er moment; in both cases, the changes in $4f$ spin magnetism are associated with lowering the total energy in their respective structures. Similar to the $4f$ moment magnetism, the higher spin polarization of $5d$ moments is controlled by Dy in the tetragonal and by Er in the orthorhombic $Er_{0.75}Dy_{0.25}Co_2$ [Figs. 4(a)–4(c)].

The anisotropic energy density relation (energy density expansion within the framework of spherical harmonic approximation): $\frac{E_a}{V} \approx \frac{\kappa_2}{2}(3\cos^2\theta - 1) + \frac{\kappa_4}{8}(35\cos^4\theta - 30\cos^2\theta + 3)$ [31–33] provides anisotropic energy landscapes, where κ_2 (second-order) and κ_4 (fourth-order) coefficients are products of the corresponding quadrupolar/octupolar moments and crystal-field parameters within the crystal environment. To make anisotropy calculations feasible, we treated $Er_{1-x}Dy_x$ as a pseudo-atom with $4f$ electrons between Dy ($4f^9$) and Er ($4f^{11}$) in $Er_{1-x}Dy_xCo_2$. The anisotropic energy landscape calculated by including only κ_2 shows uniaxial anisotropy [31] [Figs. 4(d)–4(f)] supporting tetragonal distortion in $Er_{1-x}Dy_xCo_2$ ($x = 0.25, 0.5$, and 0.75). On the other hand, the anisotropic energy landscape calculated by including both coefficients for $Er_{0.75}Dy_{0.25}Co_2$ adopts quite different dumbbell-like shape indicating easy plane anisotropy [Fig. 4(d')]. The dumbbell shape shrinks vertically and expands around the

equator for $Er_{0.5}Dy_{0.5}Co_2$ [Fig. 4(e')] suggesting a diminishing orthorhombic distortion as x increases. However, calculations show easy cone [31] anisotropy (tetragonal distortion) for $Er_{0.25}Dy_{0.75}Co_2$ [Fig. 4(f')] indicating the possibility of canted magnetism.

IV. CONCLUSIONS

In conclusion, we demonstrate that $Er_{1-x}Dy_xCo_2$ undergoes two magnetostructural transitions when $x = 0.25$: a first-order cubic to tetragonal at T_C followed by a second-order tetragonal to an unconventional body-centered orthorhombic *Imma* structure. The ground-state *Imma* structure has been confirmed both experimentally and from first-principles calculations. Although the volume changes at the first-order transition in both $Er_{0.75}Dy_{0.25}Co_2$ and $Er_{0.5}Dy_{0.5}Co_2$ are practically identical, the tetragonal structure is more stable in $Er_{0.5}Dy_{0.5}Co_2$ where no orthorhombic distortion is observed, but multiple magnetic transformations persist when $0.25 \leqslant x \leqslant 0.75$. Calculations suggest that coupled with strong 4f-5d-3d hybridization, Dy magnetism underpins the stability of the tetragonal distortion, whereas Er magnetism is mainly responsible for the emergent orthorhombic structure in $Er_{0.75}Dy_{0.25}Co_2$. The complexity observed in $Er_{1-x}Dy_xCo_2$ system is truly unexpected as it arises from the competition between rare-earth sublattices of two next-near-neighbors in the periodic table (Dy and Er) randomly occupying crystallographically indistinguishable lattice sites. Apparently, a 3:1 mixture of Er and Dy in $Er_{0.75}Dy_{0.25}Co_2$ closely mimics the $4f^{10}$ states of Ho, in effect "averaging" the $4f^9$ states of Dy and $4f^{11}$ states of Er. Our results clearly demonstrate that one can recreate the unique crystal structure and physical properties of a 4f-based compound with a combination of two different rare-earth metals, in the same way that Sm-type crystal structure is created by mixing Nd and Tb or Pr and Dy at specific concentrations [34]. The results reported here, therefore, call for re-evaluation of our understanding of the chemistry and physics of continuous solid solutions involving mixed lanthanide alloys and compounds. We expect similar phenomena waiting to be discovered in numerous other mixed 4f electron systems, potentially leading to many more examples of heretofore unknown multiple structural and magnetic phase transformations in systems thought to be of little interest based on known structure and properties of parent binary compounds.

ACKNOWLEDGMENTS

The Ames Laboratory is operated for the U. S. Department of Energy (DOE) by Iowa State University of Science and Technology under contract No. DE-AC02-07CH11358. This work was supported by the Office of Science of the U.S. DOE, Division of Materials Sciences and Engineering, Office of Basic Energy Sciences.

[1] J. Jensen and A. K. Mackintosh, *Rare Earth Magnetism* (Clarendon, Oxford, 1991), pp. 286–304.
[2] I. D. Hughes, M. Däne, A. Ernst, W. Hergert, M. Lüders, J. Poulter, J. B. Staunton, A. Svane, Z. Szotek, and W. M. Temmerman, Nature (London) **446**, 650 (2007).
[3] F. Laves and K. Löhberg, Math. Phys. K1. IV, Neue Folge 1, Nr. **6**, 59 (1934).
[4] K. A. Gschneidner, Jr. and V. K. Pecharsky, Z. Kristallogr. **221**, 375 (2006).
[5] R. Huang, Y. Liu, W. Fan, J. Tan, F. Xiao, L. Qian, and L. Li, J. Am. Chem. Soc. **135**, 11469 (2013).
[6] A. P. Ramirez, B. S. Shastry, A. Hayashi, J. J. Krajewski, D. A. Huse, and R. J. Cava, Phys. Rev. Lett. **89**, 067202 (2002).
[7] M. Kobayashi and H. Tanaka, Nat. Commun. **7**, 13438 (2016).
[8] F. Guillou, G. Porcari, H. Yibole, N. V. Dijk, and E. Brück, Adv. Mater. **26**, 2671 (2014).
[9] K. A. Gschneidner, Jr., Y. Mudryk and V. K. Pecharsky, Scripta Mater. **67**, 572 (2012).
[10] C. Dong, C. Chen, K. Asokan, C. Chang, Y. Chen, J. Lee, and J. Guo, Langmuir **25**, 7568 (2009).
[11] N. V. Baranov, A. A. Yermakov, A. N. Pirogov, A. V. Proshkin, S. N. Gvasaliya, and A. Podlesnyak, Phys. Rev. B **73**, 104445 (2006).
[12] J. Zou, D. Paudyal, J. Liu, Y. Mudryk, V. K. Pecharsky, and K. A. Gschneidner, Jr., J. Mater. Chem. C **3**, 2422 (2015).
[13] Y. Mudryk, V. K. Pecharsky, and K. A. Gschneidner, Jr., Influence of an applied magnetic field on the structural transition in RCo_2 (R = Dy, Ho, Er) compounds, in *Proceeding of 3rd. International Conference on Magnetic Refrigeration at Room Temperature, Des Moines, Iowa, USA, May 11–15, 2009*, edited by P. W. Egolf (International Institute of Refrigeration, Des Monies, 2010), p. 127.
[14] V. K. Pecharsky, K. A. Gschneidner, Jr., Y. Mudryk, and D. Paudyal, J. Magn. Magn. Mater. **321**, 3541 (2009).
[15] K. Morrison, A. Dupas, Y. Mudryk, V. K. Pecharsky, K. A. Gschneidner, Jr., A. D. Caplin, and L. F. Cohen, Phys. Rev. B **87**, 134421 (2013).
[16] Y. Mudryk, D. Paudyal, A. K. Pathak, V. K. Pecharsky, and K. A. Gschneidner, Jr., J. Mater. Chem. C **4**, 4521 (2016).
[17] A. H. King, R. G. Eggert, and K. A. Gschneidner, Jr., in *The Rare Earths as Critical Materials in Handbook on the Physics and Chemistry of Rare Earths*, edited by J. C. G. Bunzli and V. K. Pecharsky (North-Holland, Amsterdam, New York, Oxford, 2016), Vol. 50, p. 19.
[18] Materials Preparation Center, Ames Laboratory of US, DOE, Ames, IA, USA, www.mpc.ameslab.gov.
[19] A. P. Holm, V. K. Pechasky, K. A. Gschneidner, Jr., R. Rink, and M. N. Jirmanus, Rev. Sci. Instrum. **75**, 1081 (2004).
[20] B. Hunter, Rietica-A Visual Rietveld Program, International Union of Crystallography Commission on Powder Diffraction Newsletter No. 20, (Summer, 1998), http://www.rietica.org.
[21] V. K. Pecharsky, J. O. Moorman, and K. A. Gschneidner, Jr., Rev. Sci. Instrum. **68**, 4196 (1997).
[22] V. I. Anisimov, F. Aryasetiawan, and A. I. Lichtenstein, J. Phys.: Condens. Matter **9**, 767 (1997).
[23] O. K. Andersen and O. Jepsen, Phys. Rev. Lett. **53**, 2571 (1984).

[24] P. Blaha, K. Schwarz, G. Madsen, D. Kvasnicka, and J. Luitz, *WIEN2k, An Augmented Plane Wave + Local Orbitals Program for Calculating Crystal Properties* (Karlheinz Schwarz, Techn. Universität Wien, Austria, 2001).

[25] D. Paudyal, A. K. Pathak, V. K. Pecharsky, and K. A. Gschneidner, Jr., J. Phys.: Condens. Matter **25**, 396002 (2013).

[26] R. M. Moon and W. C. J. Koehler, J. Appl. Phys. **36**, 978 (1965).

[27] K. Parlinski and P. Zielinski, Z. Phy. B Condens. Matter **44**, 317 (1981).

[28] V. K. Pecharsky, A. P. Holm, K. A. Gschneidner, Jr., and R. Rink, Phys. Rev. Lett. **91**, 197204 (2003).

[29] V. K. Pecharsky, J. Cui, and D. D. Johnson, Phil. Trans. R. Soc. A **374**, 20150305. (2016).

[30] A. Arrott, Phys. Rev. **108**, 1394 (1957)

[31] R. Skomski, *Simple Models of Magnetism* (Oxford University Press, Oxford, 2006), Chap. 3, p. 79 and references therein.

[32] A. J. Freeman and R. E. Watson, Phys. Rev. **127**, 2058 (1962).

[33] P. Fulde, Crystal Fields in *Handbook on the Physics and Chemistry of Rare Earths*, edited by K. A. Gschneidner, Jr. and L. Eyring (North-Holland, Amsterdam, New York, Oxford, 1979), Vol. 2, p. 295.

[34] K. A Gschneidner, Jr., J. Less-Common Metals **114**, 29 (1985).